Cell Reports
Article

Charting Monosynaptic Connectivity Maps by Two-Color Light-Sheet Fluorescence Microscopy

Christian J. Niedworok,[1] Inna Schwarz,[1] Julia Ledderose,[1] Günter Giese,[2] Karl-Klaus Conzelmann,[3] and Martin K. Schwarz[1,*]
[1]Department of Molecular Neuroscience
[2]Department of Biomedical Optics
Max Planck Institute for Medical Research, Jahnstrasse 29, D-69120 Heidelberg, Germany
[3]Max von Pettenkofer-Institute and Gene Center, Ludwig-Maximilians- University, Munich D-81377, Germany
*Correspondence: mschwarz@mpimf-heidelberg.mpg.de
http://dx.doi.org/10.1016/j.celrep.2012.10.008

SUMMARY

Cellular resolution three-dimensional (3D) visualization of defined, fluorescently labeled long-range neuronal networks in the uncut adult mouse brain has been elusive. Here, a virus-based strategy is described that allowed fluorescent labeling of centrifugally projecting neuronal populations in the ventral forebrain and their directly, monosynaptically connected bulbar interneurons upon a single stereotaxic injection into select neuronal populations. Implementation of improved tissue clearing combined with light-sheet fluorescence microscopy permitted imaging of the resulting connectivity maps in a single whole-brain scan. Subsequent 3D reconstructions revealed the exact distribution of the diverse neuronal ensembles monosynaptically connected with distinct bulbar interneuron populations. Moreover, rehydratation of brains after light-sheet fluorescence imaging enabled the immunohistochemical identification of synaptically connected neurons. Thus, this study describes a method for identifying monosynaptic connectivity maps from distinct, virally labeled neuronal populations that helps in better understanding of information flow in neural systems.

INTRODUCTION

Visualization of direct long-distance connections between fluorescently labeled neuronal clusters in the adult, intact mouse brain has not yet been feasible. Usually, a source population of neurons is labeled by local injection of neuroanatomical tracers to visualize their projections, only sampling connections between regions (Cowan, 1998). Although providing useful information, most approaches mark a cell's neurites but not the synaptically connected cellular targets (Katz et al., 1984; Swanson, 2000). Genetically targeted tracers such as wheat germ agglutinin, barley lectin, or tetanus toxin c-fragment, which can undergo transsynaptic transport, are an alternative, although the analysis of directionality is complex (Braz et al., 2002; Horowitz et al., 1999; Yoshihara et al., 1999; Kissa et al., 2002; Köbbert et al., 2000). Moreover, these tracers are nonreplicating and thus undergo dilution at each synapse, which considerably limits the number of detectable connections. Recently, the use of virus-based transsynaptic tracer systems has greatly facilitated the identification of synaptically connected neurons over long distances (Lundh, 1990; Kim et al., 1999; Astic et al., 1993; Bak et al., 1977; Wickersham et al., 2007a, 2007b; Beier et al., 2011; Lo and Anderson, 2011).

Microscopic analysis of these long-range connectivity maps usually involves sectioning the brain and imaging every individual section. A perfect alignment of the sections is almost impossible due to slicing artifacts, resulting in a loss of spatial information. Hence, an undistorted 3D reconstruction is only available from within individual slices, effectively limiting the reconstruction depth to, at best, ~300 μm using standard confocal microscopy and ~800 μm using two-photon microscopy, thus complicating circuit analysis (Helmchen and Denk, 2005).

An alternative to slicing the brain is the preparation of flattened hemibrains for circuit reconstructions, a technique that can only be used to analyze projections close to the surface of the brain (Sosulski et al., 2011). Imaging of the flattened brain preparation is possible but, again, limited in depth. Furthermore, flattening considerably distorts the 3D connectivity matrix (Sosulski et al., 2011). This is a considerable problem, since the 3D architecture of long-range projections, which often run deep, is crucial for generating comprehensive connectivity maps (Helmstaedter et al., 2008; Bohland et al., 2009).

In summary, an undistorted 3D reconstruction of neuronal circuits at confocal resolution is only possible from within a single slice or a flat-brain preparation, significantly complicating large circuit analysis. Notably, new methods termed serial two-photon tomography and micro-optical section tomography also aim to overcome these problems; however, these methods are still hampered by low acquisition speed and only allow us to run one single undistorted scan per sample. Thus, if the first scan fails, it is not possible to rescan the sample (Li et al., 2010; Ragan et al., 2012).

This study presents a combinatorial approach that allows multiple imaging sessions of stereotaxically targeted, virus-labeled monosynaptically connected neuronal circuits in undistorted whole-brain preparations. This experimental strategy enables the generation of comprehensive 3D network reconstructions

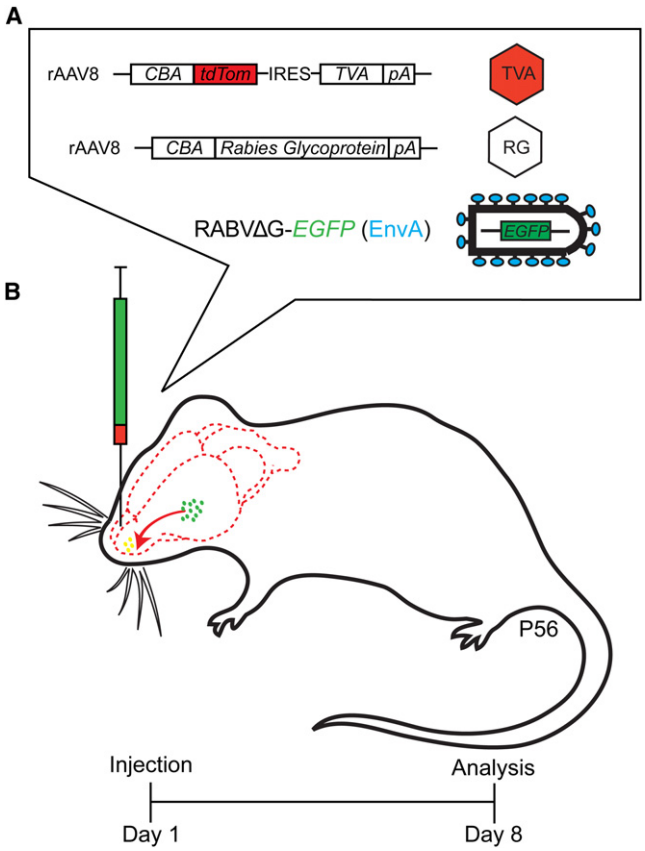

Figure 1. Stereotaxic Virus Delivery into the Olfactory Bulb of Adult Mice

(A) Schematic showing the different viruses used for stereotaxic injections. Two rAAVs subtype 8, one expressing tdTomato linked with an IRES to *TVA*, the other expressing rabies glycoprotein, both under control of a *CBA* promoter, are mixed with an EnvA pseudotyped, glycoprotein-gene deleted rabies virus expressing EGFP (RABVΔ*G-EGFP* [EnvA]).

(B) Schematic showing the stereotaxic injection of the virus cocktail into the main OB of an adult mouse (p56) and the timeline from injection to analysis (bottom). The needle of a syringe (green: RABVΔ*G-EGFP* [EnvA], red: rAAV mix) is inserted into the mouse brain (dashed red lines) at the level of the OB. Yellow dots represent the source cell population. Green dots indicate directly connected (red arrow) presynaptic neurons. See also Figure S1. rAAV, recombinant adenoassociated virus; *CBA*, chicken beta-actin promoter/enhancer; IRES, internal ribosomal entry site; tdTomato, tandem dimer Tomato red-fluorescent protein; RABVΔ*G-EGFP* (EnvA), glycoprotein gene-deficient, EGFP expressing rabies virus encapsulated with the avian sarcoma and leukosis virus envelope protein EnvA; TVA, tumor virus A; p56, postnatal day 56.

at cellular resolution. Neural circuits are fluorescently labeled using a single-injection protocol based on previously published rabies virus-mediated, monosynaptically restricted, retrograde transsynaptic tracing (Wickersham et al., 2007b; Miyamichi et al., 2011; Osakada et al., 2011; Rancz et al., 2011). After optical clearing using a protocol that allows for reliable two-color fluorescent protein preservation in adult brain tissue, the intact brain is imaged using an improved light-sheet microscopy method. Moreover, after 3D image acquisition, the cleared brains can be rehydrated, which reverses the clearing procedure while preserving the fluorescent proteins. Rehydrated brains can subsequently be sectioned followed by regular antibody staining and imaging. To test the validity of this experimental approach in a well-described system, we backtraced neurons that centrifugally innervate diverse interneuron populations in the murine main olfactory bulb (OB).

The OB is known to receive a substantial number of projection fibers from distinct regions of the ventral forebrain, and the abundance of these centrifugal fibers suggests that information processing in the OB is influenced by this input (Mouret et al., 2009; Strowbridge, 2009; Isaacson, 2010; Kiselycznyk et al., 2006). These centrifugal fibers can be divided into two groups according to their origin. One fiber group comes from the olfactory cortex, which receives reciprocal input from the OB. Fibers from the other group come mainly from cerebral nuclei known to release neuromodulators, such as acetylcholine (ACh), serotonin (5-HT), and noradrenaline (Matsutani and Yamamoto, 2008; Matsutani, 2010).

Current data on number and spatial distribution of neurons centrifugally projecting into the mouse OB are relatively rare (Carson, 1984b) and do not allow a direct comparison of the number and the spatial distribution of distinct neuronal populations monosynaptically connected to defined groups of bulbar interneurons. However, given the abundance of centrifugal fibers, an accurate account of number and spatial distribution of projection neurons is necessary to weigh their contribution to interneuron modulation within the OB.

To address this issue, we modified rabies viruses (RABV) in conjunction with recombinant adenoassociated viruses (rAAVs) and backtraced the neuronal populations that are monosynaptically connected to either periglomerular or granule cells in the OB. The resulting fluorescently labeled connectivity maps were then imaged by high-resolution fluorescence microscopy and further analyzed utilizing a home-built light-sheet fluorescence microscope system (LSFM). These results provide a omplete high-resolution 3D map of the different neuronal populations in the forebrain that are directly connected to interneurons in distinct layers of the main OB. Closer inspection suggests that the number and spatial distribution of neurons projecting from basal cerebral nuclei is presently underestimated (Carson, 1984b). Centrifugally projecting neurons from cerebral forebrain nuclei include the entire diagonal band of Broca (DBB). Moreover, the number of centrifugal inputs emanating from the DBB is higher compared to that from piriform cortex (PC). Collectively, these studies present a methodological approach revealing unexpected monosynaptic connections between inhibitory bulbar interneurons and centrifugally projecting neurons from the DBB.

RESULTS

rAAV-Dependent, Monosynaptic Retrograde Labeling of Centrifugal Olfactory Projections

To efficiently label monosynaptically connected neuronal ensembles in the adult mouse brain, a modified rabies virus (RABV) in conjunction with rAAVs was used (Figure 1A). Both virus types efficiently infect neurons and both, our data and published results showed no notable effects on morphology or physiology over the periods analyzed in this study (Ugolini, 2010; Luo et al., 2008).

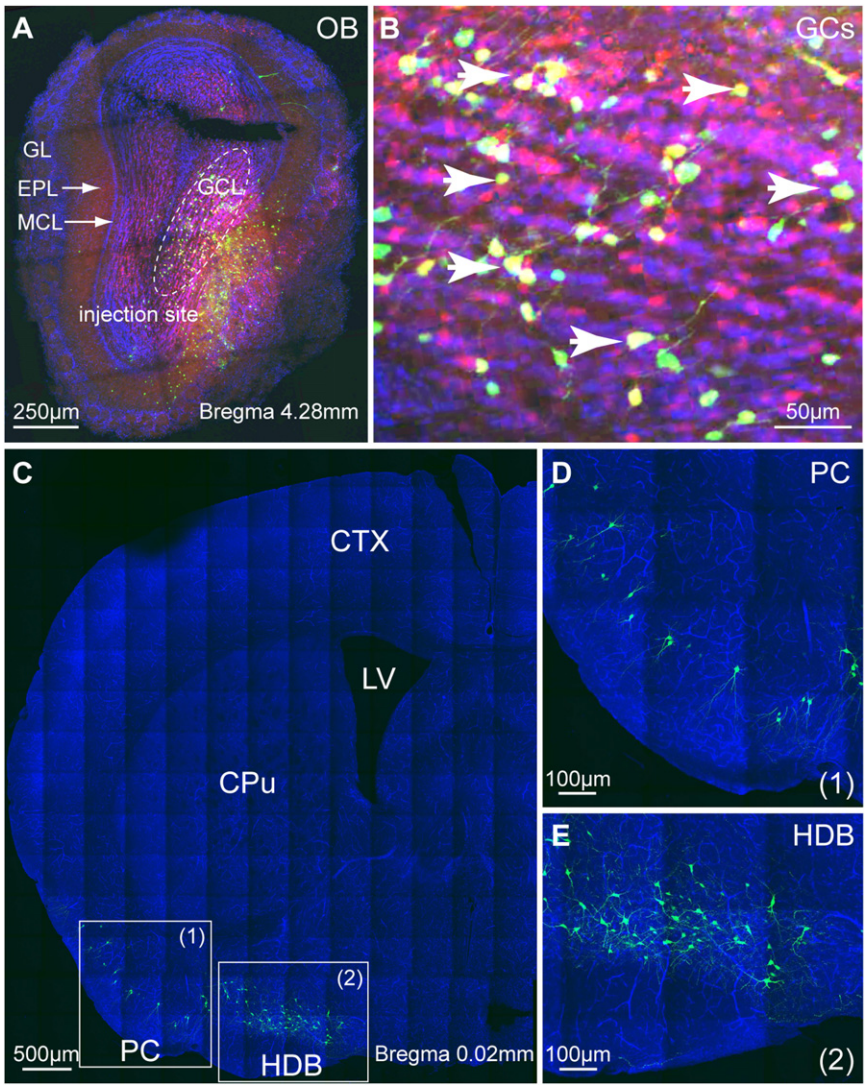

Figure 2. RABV Spread after Stereotaxic Delivery into the Main OB

(A) Confocal mosaic image of a coronal section from the OB of an adult mouse 8 days after virus-cocktail delivery. White dotted ellipse marks the point of virus delivery in the GCL. White arrows point at the different layers (GL, EPL, MCL) of the OB. Blue: DAPI fluorescence. Double-infected tdTomato and EGFP expressing neurons appear in yellow. Red neurons express tdTomato only. Green RABV-infected neurons express EGFP only.

(B) High magnification of double-infected neurons (exemplary white arrows) in the GCL from (A).

(C) Confocal mosaic image of a coronal section through the brain (Bregma 0.02 mm) of an adult mouse after virus-cocktail delivery into OB. PC (1) and HDB (2) are marked by white squares and contain numerous RABV-infected, EGFP-positive neurons.

(D and E) Closeup of (1) and (2) from (C). Note the high density of EGFP-positive neurons in HDB (E). See also Figures S2, S3, and S4. Blue: DAPI fluorescence; OB, olfactory bulb; GCL, granule cell layer; GL, glomerular layer; EPL, external plexiform layer; MCL, mitral cell layer; CTX, cerebral cortex; CPu, caudate putamen; LV, lateral ventricle; HDB, horizontal limb of the diagonal band; PC, piriform cortex.

The modified RABV selectively infects neurons expressing the EnvA receptor tumor virus A (TVA), and expresses either enhanced green fluorescent protein (EGFP) or mCherry (Wickersham et al., 2007a, 2007b; Osakada et al., 2011). To control spatiotemporal infection of target neurons and transsynaptic transport of this modified RABV, two rAAVs were coinjected. The fact that the majority of neurons express both EGFP and tdTomato after coinjection of two viruses shows that rAAV8 is capable of efficiently coinfecting individual neurons (Figure S1). One rAAV encodes the TVA receptor, necessary for initial RABV infection, coupled to a fluorescent marker protein allowing the visualization of target neurons. The other rAAV encodes RABV glycoprotein (RG) allowing transsynaptic transport of the modified RABV (Figure 1A). After transcomplementation in triple-infected neurons, the RABV crosses synapses in a strictly retrograde fashion and labels only directly connected, presynaptic partner neurons (Wickersham et al., 2007a, 2007b). If these transsynaptically infected neurons are outside of the rAAV-infected area, they lack RG expression, and hence the modified RABV is trapped and cannot spread further. Note that the accuracy and efficacy of transsynaptic tracing is greatly improved by delivering a cocktail of both rAAVs together with the modified RABV in a single stereotaxic injection (Figure 1B). The neurons coinfected by all three viruses are referred to as "source neurons."

The OB receives a vast amount of fibers, originating from different cortical and subcortical regions (Figures S2A–S2D). Most importantly, although direct synaptic connections between inhibitory bulbar interneurons and centrifugally projecting cortical neurons have been identified, an accurate estimate of the different dispersed, monosynaptically connected cell populations is still missing (Wilson and Mainen, 2006; Balu et al., 2007; Gao and Strowbridge, 2009). To selectively identify these populations and to compare their numbers, a rAAV-RABV "cocktail" (see Extended Experimental Procedures) was stereotaxically injected into the granule cell layer (GCL) of the main OB (Figure 2, n = 10 mice).

This resulted in efficient and selective RABV-driven EGFP expression in rAAV-infected tdTomato/TVA expressing source neurons in the OB (yellow) (Figures 2A and 2B), as well as retrograde synaptically connected partner neurons in cortical and subcortical regions (green) 8 days after injection (Figures 2C–2E). Yellow starter neurons, coexpressing tdTomato and EGFP, could readily be identified (Figure 2B). In contrast, presynaptic, retrogradely connected partner neurons are solely infected by modified RABV and therefore express EGFP only

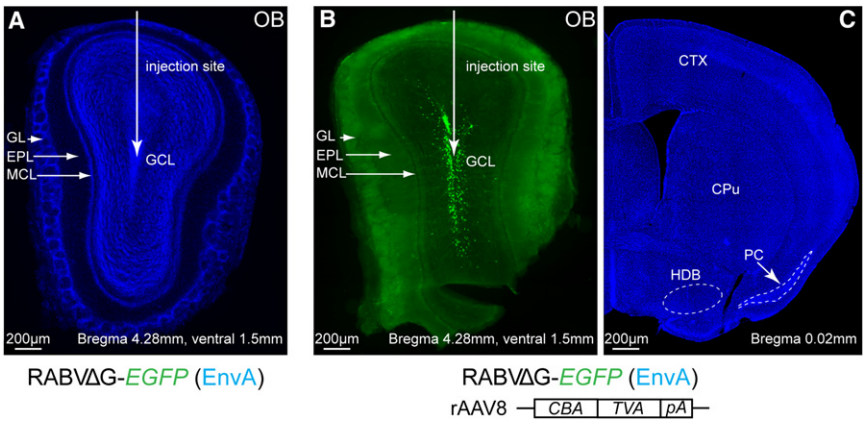

Figure 3. TVA Receptor and Rabies Glycoprotein Dependency of Modified RABV Infection

(A) Fluorescence image of a 70 µm coronal section from the OB of an adult mouse injected with an EnvA pseudotyped, glycoprotein gene-deleted rabies virus expressing EGFP (RABVΔ*G-EGFP* [EnvA]) (bottom). DAPI fluorescence appears in blue. White arrow from top points at stereotaxic injection site. White arrows from left point at different layers (GL, EPL, MCL) of the OB. No EGFP-positive cells were found.

(B) Fluorescence image of a 70 µm coronal section from the OB of an adult mouse injected with a virus cocktail containing an rAAV expressing the TVA receptor and the EnvA pseudotyped, glycoprotein gene-deleted rabies virus expressing EGFP (RABVΔ*G-EGFP* [EnvA] [bottom]). The white arrow from the top points at the injection site containing numerous EGFP-labeled (green) neurons. The white arrows from the left point at different layers of the OB.

(C) Fluorescence image of a 70 µm coronal section through the brain (Bregma 0.02 mm) of an adult mouse injected into the OB with a virus cocktail containing an rAAV expressing the TVA receptor and the EnvA pseudotyped, glycoprotein-deleted, RABV-expressing EGFP (RABVΔ*G-EGFP* [EnvA]).

Blue: DAPI fluorescence. HDB and PC are encircled (white dotted lines). No EGFP-positive (green) neurons can be detected.

(green) (Figures 2C–2E). EGFP-positive neurons were detected in the anterior olfactory nucleus (data not shown), the PC (Figures 2C and 2D), and abundantly in the horizontal limb of the diagonal band (HDB) (Figures 2C and 2E). Since these results were present in all injected mice, we surmise that after coinjection, the pseudotyped RABV remains sufficiently intact in living brain tissue to infect rAAV-infected neurons expressing the TVA receptor, and is able to traverse synapses in a retrograde manner after RG *trans*-complementation. Interestingly, although GCs are extensively connected with mitral cells (MCs) via reciprocal dendrodendritic synapses, RABV-positive, presynaptic MCs could not be identified (Figure S3 and Discussion).

As expected, no fluorescent neurons were found upon injection of modified RABV alone into the OB, indicating that infection of neurons with the modified RABV is strictly dependent on TVA receptor expression (Figure 3A, n = 9 mice). Similarly, coinjection of modified RABV with rAAVs expressing TVA into the GCL resulted in selective infection of source neurons in the GCL (Figure 3B, n = 6 mice). Note that no EGFP-positive neurons could be found in PC or HDB, indicating that transsynaptic RABV transport is strictly dependent on RG expression (Figure 3C). Since no EGFP-positive, RABV-infected cells were found among MCs, interneurons in the external plexiform layer (EPL), or periglomerular cells (PGCs), these data demonstrate that the source cell population is confined to the injection site in the GCL. Note that in these experiments the observed postsynaptic neurons showed regular morphology. However, after prolonging the exposure to the virus cocktail to more than 15 days, EGFP-positive glia cells and isolated neurons with distorted morphology appeared in the virus cocktail-infected areas (Figure S4).

Collectively, these experiments illustrate efficient triple infection of source neurons upon a single stereotaxic injection with subsequent transsynaptic labeling of monosynaptically connected neurons and validate this strategy for virus-mediated, retrograde monosynaptic tracing in vivo. More specifically, OB GCs receive monosynaptic input selectively from neurons in the PC and HDB. Yet, an exact estimation of the spatial expansion of the different brain regions connected to the pool of source neurons is difficult and time consuming when only based on representative coronal sections.

Virus-Labeled Connectivity Maps Can Be Visualized by Light-Sheet Microscopy in the Intact Adult Mouse Brain

To assess the exact topography of monosynaptic afferent connectivity maps, the improved RABV vector system was combined with a refined light-sheet fluorescence microscopy technique. The feasibility of the imaging strategy was first tested by stereotaxically injecting the source virus cocktail unilaterally into the anterior olfactory nucleus (AON) to label the neuronal ensembles presynaptic to this structure. Eight days later, the brains (n = 3 mice) were cleared using a modified protocol (see Experimental Procedures) based on a published clearing procedure (Dodt et al., 2007). This method enabled us to reduce the opacity of the brain tissue to a point where it became almost completely transparent, while preserving much of the EGFP fluorescence (Figures 4A–4F). The procedure also caused the tissue to uniformly shrink by ~25% in each dimension. Subsequently, the entire brain was imaged using a custom-built LSFM (see Experimental Procedures).

As shown in Figure 4G, the brain is illuminated from one side with a thin sheet of light, generated by a laser and beam-shaping optics, and scanned through an excitation objective. The light emitted from the sample is then captured by a detection objective placed above the sample perpendicular to the illumination plane. This experimental setup allowed imaging of a complete frame within a single 50–300 ms exposure. Note that photobleaching of the sample is significantly reduced in light-sheet fluorescence microscopy compared to standard confocal microscopy, due to illumination of only the actively imaged plane, with virtually no illumination of structures out of focus. This strategy allowed imaging of directly connected neuronal populations in the olfactory system of adult mice in an unsliced brain, resulting in a single undistorted data set containing all neuronal populations of interest (Figure 5). Bright EGFP

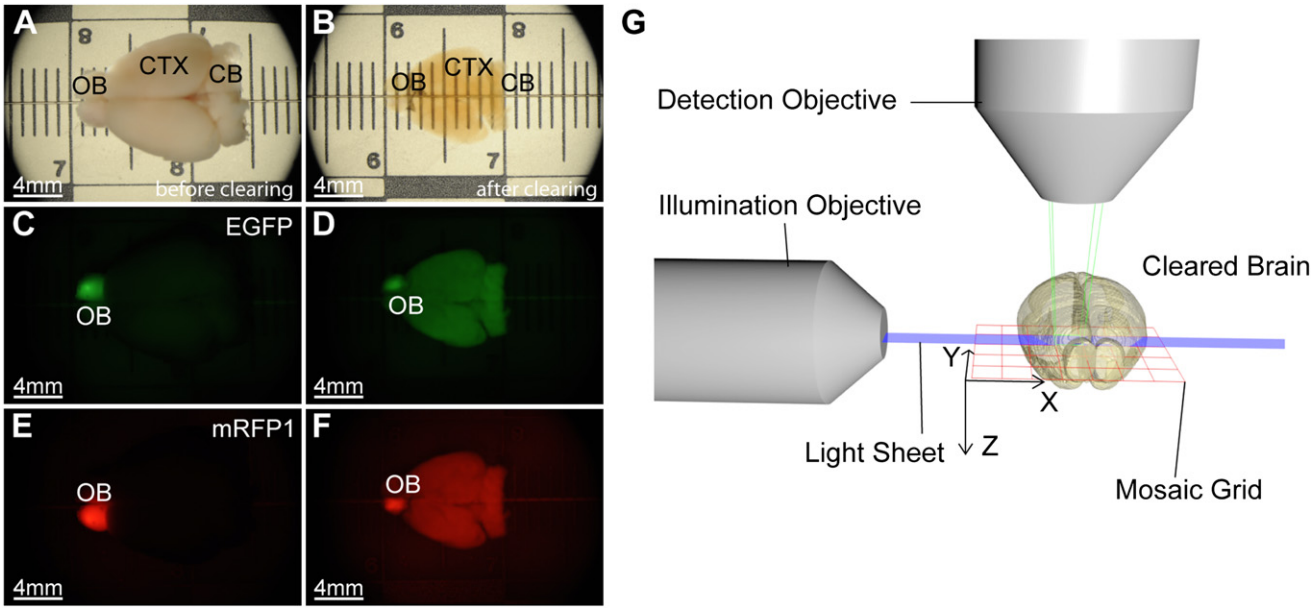

Figure 4. Preservation of EGFP and mRFP1 Fluorescence after Optical Clearing and Light-Sheet Fluorescence Microscopy Principle

(A) Picture of a perfused mouse brain 8 days after stereotaxic injection of rAAV-*CBA-EGFP* IRES *TVA* in the right, and *rAAV-CBA-mRFP1 IRES TVA* the left OB (injection volume: 300 nl each, Bregma: 4.28 mm, lateral: 0.5 mm, ventral: 2.5 mm).

(B) Picture of the same brain after optical clearing for light-sheet microscopy.

(C) Uncleared brain revealing bright EGFP fluorescence (green) in right OB.

(D) Cleared brain revealing preservation of EGFP fluorescence (green) in right OB.

(E) Uncleared brain revealing bright mRFP1 fluorescence (red) in left OB.

(F) Cleared brain revealing bright mRFP1 fluorescence (red) in left OB.

(G) Schematic illustrating the principle of light-sheet fluorescence microscopic imaging. The cleared mouse brain is placed under a detection objective and illuminated from one side with the light sheet (blue) generated by scanning through an illumination objective. The brain is moved in x, y, z directions to generate a virtual mosaic grid (red).

(A)–(F) Images taken with a dissecting microscope in *trans*-/epi-illumination (A), transillumination (B), green fluorescence (C and D), or red fluorescence mode (E and F). See also Movie S1. EGFP, enhanced green fluorescent protein; mRFP1, monomeric red fluorescent protein 1.

fluorescence from modified RABV-infected neurons was visible in several different cortical and subcortical structures (Figures 5A–5D). These results clearly show that 8 days after a single virus-cocktail injection, modified RABV-driven EGFP expression levels are sufficient to allow light-sheet fluorescence microscopic imaging of whole brains after tissue clearing. The sampling resolution (6.7 μm/pixel) was sufficient to identify the axonal bundles of the anterior commissure (Figure 5D), which connects the ipsi- and contralateral AONs. rAAV-driven red tdTomato fluorescence, labeling the source neurons, was lost during the clearing protocol, which prevented a distinction between primary infected postsynaptic, and directly connected presynaptic neurons.

Two-Color Light-Sheet Microscopic Imaging of Centrifugal Monosynaptic Olfactory Circuits

To reliably identify the spatially defined postsynaptic source cell population and thus allow an appropriate sampling of monosynaptically connected neurons, different red-shifted fluorescent proteins were tested (mCherry, dtTomato, and mRFP1) for their ability to emit fluorescence after optical clearing. The signal of tdTomato was completely lost during clearing and mCherry fluorescence was only very faintly detectable. mRFP1 turned out to be the only red fluorescent protein, which was detectable 8 days after stereotaxic delivery and also remained sufficiently stable for LSFM imaging after optical clearing (Figures 4E and 4F). To image the neuronal populations that are directly connected with interneurons within the GCL, the virus cocktail was stereotaxically injected into the GCL of the OB (n = 4 mice). Eight days later, the brains were cleared for LSFM imaging. To further improve the optical resolution in whole-brain LSFM scans (tested down to 639 nm/pixel, see Experimental Procedures), an automated acquisition of mosaic images was implemented. In addition, a custom ImageJ plug-in was written to facilitate the stitching and handling of these large data sets (tested up to 213 GB, see Experimental Procedures), which finally allowed the visualization of an entire fluorescently labeled neuronal circuit in the uncut adult brain at cellular resolution and in two colors (Figure 6). The point of virus injection is clearly visible by bright red fluorescence emitted from the rAAV-expressed mRFP1 8 days after delivery and is confined to the GC population in the center of the OB (Figures 6A and 6B). Yellow cells coexpressing EGFP from the modified RABV represent the source cell population (Figures 6A and 6B) and receive monosynaptic input from neurons located in the PC (Figures 6A and 6C) and the DBB (Figures 6A and 6D). Projection neurons from

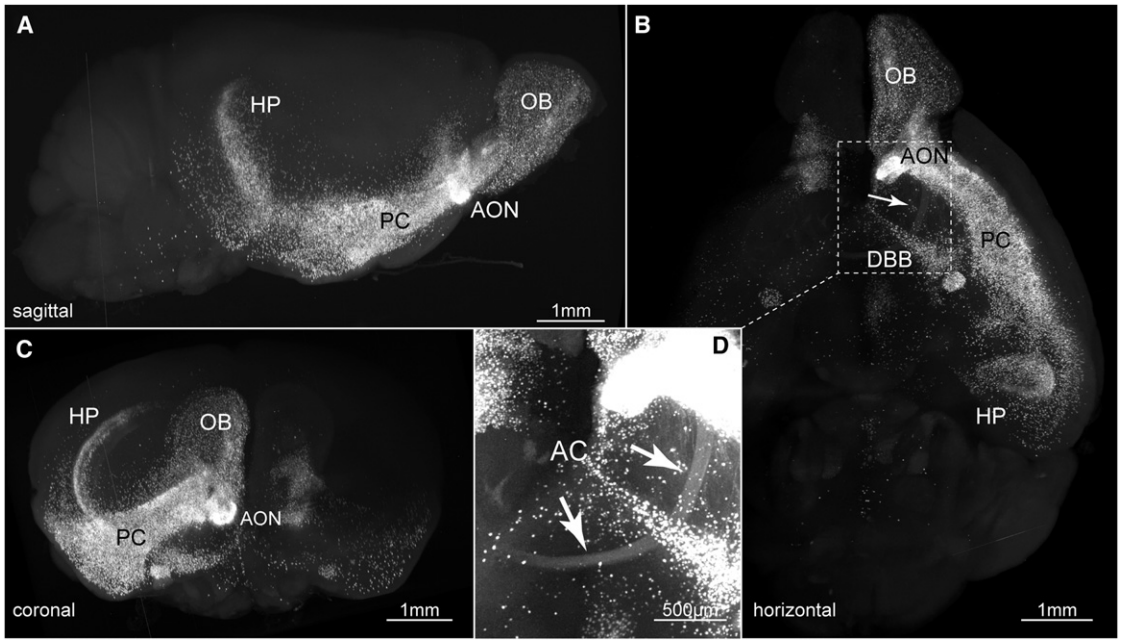

Figure 5. Light-Sheet Fluorescence Microscopic Images of RABV-Labeled Neuronal Circuits

(A–C) Maximum intensity projections of an entire mouse brain generated from a single horizontal LSFM scanning session after virus-cocktail injection into AON (0.8× detection lens; three channels recorded, only EGFP shown; x/y: 6.7 µm/pixel; z-step: 10 µm; 451 z-steps; recorded volume 9.2 × 6.9 × 4.5 mm; time 36 min; size: 3.7 GB@16 bit). RABV-infected, EGFP-positive neurons can be detected in OB and in several prominent cortical and subcortical structures (AON, PC, HP). (A) Virtual sagittal view. (B) Horizontal view. The white dotted square marks the region showing the visualization of axon bundles from AC (white arrow points at AC). (C) Virtual coronal view.

(D) Magnification of AC marked in (B). Note that the brightness was increased to improve the ACs visibility. White arrows point at the axon-bundles of AC connecting the ipsi- and contralateral AONs. CB, cerebellum; AON, anterior olfactory nucleus; AC, anterior commissure; HP, hippocampus; DBB, diagonal band of Broca.

these regions can unequivocally be identified by their bright green fluorescence. Note that none of the cells in the basal forebrain regions are mRFP1 positive and thus represent true monosynaptically connected neuronal populations (Figure 6A). Unexpectedly, after visual inspection the neurons projecting from DBB appeared to outnumber the neurons projecting from PC (Figures 6A, 6C, and 6D). To quantify these results, the number of neurons projecting from PC was counted and compared to that of neurons projecting from the DBB. This quantification revealed that, in contrast to the currently suggested 16% (Carson, 1984b), ~60% of neurons innervating a defined GCL population originate from the DBB, with the highest density of neurons in HDB. Only ~40% of neurons centrifugally innervating the same neuron population in the GCL appear to originate in PC (n = 3 mice, number of RABV-positive cells in DBB/PC: 1024/548, 1045/579, 729/536). This is important, given that the activity states of GCs are modulating the output of MCs and thus the resulting information flow into PC and amygdala (see Discussion).

Since not all centrifugal fibers terminate in the GCL but also reach the glomerular layer (GL) of the OB (Figures S2A and S2C), we next aimed at identifying the forebrain regions innervating interneurons in the GL. PGCs located in the GL of the OB are suggested to directly connect to MCs and thus, in analogy to GCs, might enhance contrast in patterned sensory processing (Aungst et al., 2003). To selectively infect PGCs, the virus cocktail was stereotaxically injected into the GL of the main OB (Figure S5). Eight days later, the virus-infected brains were subjected to optical clearing and LSFM (Figure 4, n = 4 mice). LSFM imaging revealed the extent of primary infection (red) (Figures 6E and 6F), the postsynaptic starter neurons (yellow) (Figures 6E and 6F), and the regions in the basal forebrain that are monosynaptically connected with PGCs of the OB (Figures 6E, 6G, 6H, and S6; Movie S1). 3D rendering of the LSFM data revealed the exact 3D structure of projection regions and allowed a clear separation between the different brain regions directly connected with OB PGCs (Movie S2). Interestingly, as in the case of GCs, most of the neurons directly innervating PGCs in the main OB are located in the DBB. Subsequent quantification and comparison of projection neurons from both regions revealed that in analogy to centrifugal projections onto GCs, ~65% of projection neurons onto PGCs of the OB originate in DBB (n = 4 mice, number of RABV-positive cells in DBB/PC: 1,333/793, 699/409, 1,243/514, 777/389). Collectively, these results suggest that most of the input from centrifugally projecting neurons in the basal forebrain originate in the DBB and not PC, emphasizing the contribution of centrifugal afferents from DBB in the modification of olfactory information transferred to higher cortical areas.

Immunohistochemical Identification of RABV-EGFP-Labeled Neurons in LSFM-Imaged Brains

To exactly specify the location and identity of RABV-EGFP-labeled presynaptic neurons, we established a protocol allowing the rehydratation of cleared whole-brain preparations after

LSFM imaging (see Extended Experimental Procedures). Following rehydration, the opaque brains were embedded in an agarose block and sectioned on a vibratome. As seen in Figures 7A and 7D, RABV-driven EGFP fluorescence was clearly visible, indicating successful preservation of the fluorescent protein after rehydration. The rehydrated brain sections containing the EGFP-positive, presynaptic neurons in DBB were then stained against acetocholine (Ach) to identify the cholinergic projection neurons (Figures 7B and 7E). Notably, antibody stainings produced readily detectable signals with almost no tissue background, indicating that antigens stay well preserved after rehydration and slicing of LSFM-imaged brains. Collectively, these results demonstrate successful immunohistochemical identification of RABV-labeled backtraced neurons in sections of rehydrated brains after LSFM imaging (Figures 7C and 7F).

DISCUSSION

Different virus-based systems for retrograde transsynaptic tracing have been developed and successfully applied in the systematic mapping of neuronal connections (Lundh, 1990; Kim et al., 1999; Astic et al., 1993; Bak et al., 1977; Miyamichi et al., 2011; Enquist et al., 1994; Willhite et al., 2006; Beier et al., 2011). Recently, modified rabies viruses have been developed, allowing the visualization of monosynaptically connected neurons over long distances (Wickersham et al., 2007b; Osakada et al., 2011; Rancz et al., 2011). However, a comprehensive visualization of monosynaptically connected neuronal ensembles in the entire uncut brain has not yet been implemented. So far, fluorescent circuit tracing at high precision and cellular resolution was mainly achieved in *Drosophila* and zebrafish, due to the small size and almost transparent appearance of the nervous system at early developmental stages.

This manuscript describes a strategy based on monosynaptically restricted, fluorescently labeled RABV and improved LSFM that allows comprehensive 3D mapping of monosynaptic connectivity in virtually all brain regions from unsliced whole-brain preparations. First, a RABV-mediated monosynaptic tracing method was implemented that permits labeling of select postsynaptic starter neurons in the adult mouse brain by single stereotaxic coinjection of a fluorescently tagged modified RABV and two rAAVs, one expressing a fluorescently tagged TVA receptor, the other the RABV glycoprotein. Using this approach, the entire surgical procedure was limited to a single stereotaxic injection, thus increasing the precision of source neuron targeting and reducing both the time needed to carry out a tracing experiment and the brain damage due to repeated needle insertion. This experimental setup allows fast and facile entry into various regionally defined neuronal populations. Implementation of rAAV-driven mRFP1 expression (Jach et al., 2006) to robustly label postsynaptic source neurons further allowed us to distinguish them from monosynaptically connected presynaptic partner cells starting from 8 days after infection.

In order to visualize these monosynaptic connectivity maps in the context of an entire, uncut brain at confocal resolution, we implemented a protocol that allows fluorescent protein preservation for subsequent light-sheet fluorescence microscopic imaging of adult mouse brains (see Experimental Procedures). While this optical clearing did severely reduce the fluorescence of some dyes, an issue that seemed to effect multimeric dyes, in particular, the clearing protocol allowed us to preserve the fluorescence of both EGFP and mRFP1 in the same preparation and thus facilitated an unequivocal discrimination between postsynaptic source neurons and directly connected presynaptic neurons. Unfortunately, To-Pro3 or DAPI stainings decrease with increasing imaging depths, thus complicating the assignment of fluorescently labeled neurons to defined brain structures. Improved LSFM imaging (see Experimental Procedures) allowed us to produce high-quality data of large volumes at unrivaled speed. Moreover, fluorophore intensity in cleared brain preparations remained stable for several months and even allowed repetitive reimaging.

Serial Sectioning of Rehydrated, LSFM-Imaged Brains

Although the LSFM allows comprehensive imaging of directly connected cell populations in whole-brain preparations at confocal resolution, an unequivocal identification of labeled cells has yet not been implemented. An unambiguous characterization of the specific location combined with immunohistochemical identification of traced neurons would greatly aid to a functional interpretation of imaged connectivity maps. Thus, a protocol was established that allows the rehydratation of the brains after optical clearing and LSFM imaging. Notably, the tissue and the cellular architecture, including endogenously expressed antigens and fluorescent proteins, were still intact after the clearing procedure, LSFM imaging, and rehydration, allowing for serial sectioning and subsequent immunohistochemical characterization of RABV-labeled presynaptic neurons. Thus, this technique allows us to first reveal the 3D architecture of monosynaptically connected neuronal ensembles followed by immunohistochemical characterization of connected neurons, if desired at ultrastructural resolution. If compared with serial two-photon tomography or micro-optical section tomography, this technique offers the clear advantage of allowing multiple undistorted 3D recordings while still giving the possibility to slice and further analyze the brain after 3D image acquisition using well-established staining protocols. In addition, since slicing is performed using a regular vibratome, the slices can be stored in sorted order, making it much easier to identify all slices of interest and perform a multiple-antibody staining assay (e.g., using different antibodies on successive sections).

Thus, the described protocol allows us to first clear the brain to permit high-speed 3D imaging at confocal resolution without introducing slicing artifacts, and then a reversal of the clearing procedure makes it possible to stain the previously imaged cells of interest to reveal their identity.

Synaptic Pathways Revealed by RABV-Mediated Monosynaptic Tracing and Light-Sheet Fluorescence Microscopy

The presented results allow a comparative evaluation of the contribution of different neuronal populations centrifugally innervating a common bulbar interneuron source population. Special emphasis was given to the afferent centrifugal projections from the DBB onto GCs and PGCs. Several studies already reported that the main OB is under extensive extrinsic control from PC

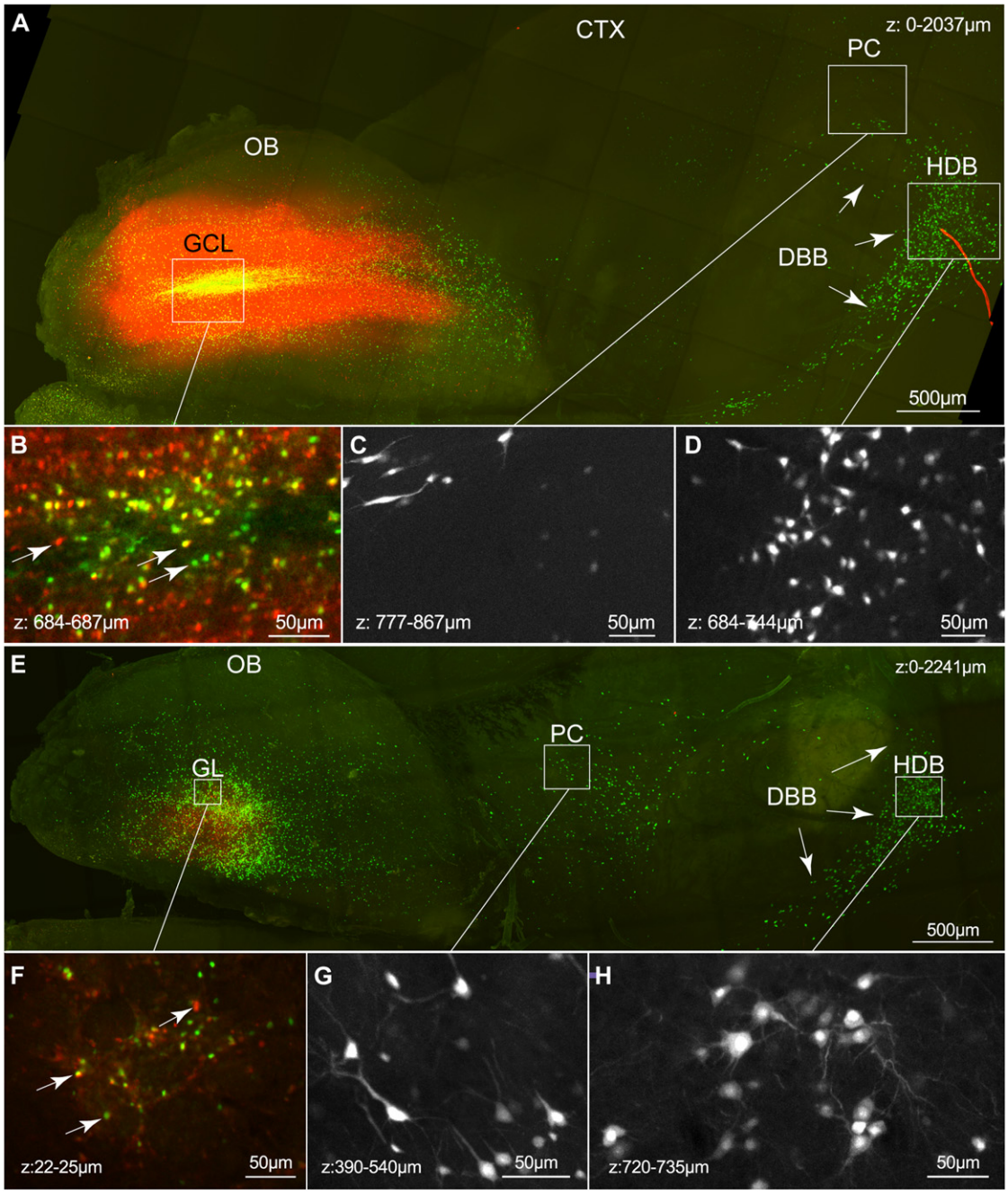

Figure 6. Light-Sheet Fluorescence Microscopic Imaging of Neuronal Populations Monosynaptically Connected with GCs or PGCs

(A–H) Maximum intensity projections generated from two horizontal LSFM mosaic scanning sessions (10× lens; two channels; x/y: 639 nm/px; z-step: 3 µm; A–D: 679 z-steps; 7 × 8 tiles; volume ~6.0 × 5.0 × 2.0 mm; E–H: 761 z-steps; 9 × 5 tiles; volume ~7.1 × 2.9 × 2.3 mm). Z ranges are measured from the highest point on the surface of the brain in the displayed area along the z axis of the viewpoint.

(A) Overview of OB and rostral forebrain. Red rAAV-infected neurons are confined to the GCL of the OB. Yellow-labeled neurons in the center of the OB represent rAAV and RABV-infected postsynaptic source neurons. Green EGFP-positive neurons in OB, PC, and DBB including HDB represent RABV-labeled presynaptic neurons, monosynaptically connected to the source cell population in OB. A red artifact is visible on the right. White squares mark the regions enlarged in (B–D).

(B) Optical section through the GCL. White arrows point at red (rAAV-infected), green (RABV-infected), and yellow (coinfected) GCs.

(C) Optical section (EGFP channel) through the PC revealing bright fluorescent neurons.

(D) Optical section (EGFP channel) through HDB revealing numerous brightly fluorescent neurons.

(E) Overview of OB and rostral forebrain. rAAV-positive neurons (red) are visible in the GL of the OB. rAAV and RABV double-infected postsynaptic source neurons (yellow) can be detected in the GL of the OB. RABV-infected neurons (green) monosynaptically connected to the source cell population can be found in OB, PC, and DBB (white arrows) including HDB. White squares mark the regions enlarged in (F–H).

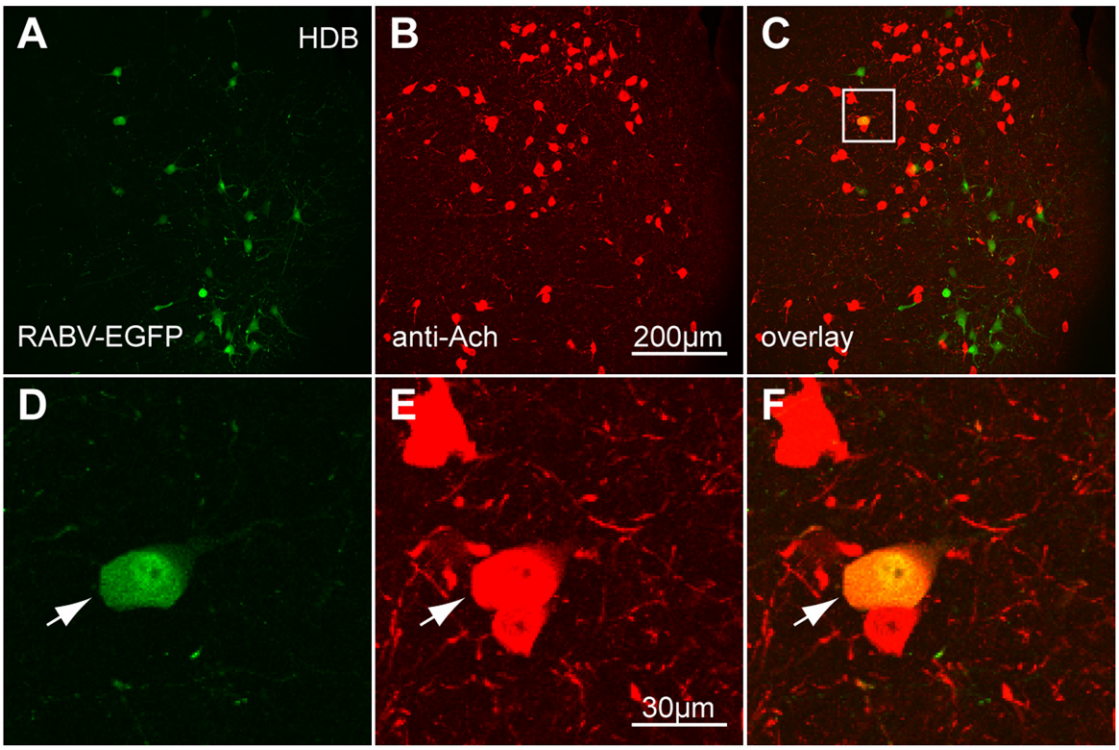

Figure 7. Preservation of EGFP Fluorescence and Antibody Staining after LSFM Imaging, Rehydratation, and Sectioning

(A) Confocal image of a 70 µm vibratome section after LSFM imaging and rehydratation showing RABV-EGFP-labeled neurons in HDB.

(B) Same section as in (A) stained against acetocholin (Ach) revealing cholinergic neurons in HDB (red).

(C) Overlay of (A) and (B) identifying cholinergic nature of RABV-labeled neurons (white rectangle).

(D–F) Magnification of the region shown in (C, white rectangle) showing a RABV-EGFP-labeled, cholinergic neuron (white arrow). See also Figure S6.

and HDB (Mouret et al., 2009; Strowbridge, 2009; Isaacson, 2010; Kiselycznyk et al., 2006; Matsutani and Yamamoto, 2008; Matsutani, 2010). Currently available results on the relative contribution of these areas suggest, however, that only ~16% of the entire centrifugal input emanates from HDB, and most of these projection neurons have been reported to be cholinergic (Carson, 1984a, 1984b; Pignatelli and Belluzzi, 2008; Cullinan and Záborszky, 1991; Kasa et al., 1995). These data indicate that the number of neurons centrifugally projecting from HDB is highly underestimated, as is the spatial extent of this projection region. In fact, our experiments show that the majority of the monosynaptic centrifugal input onto olfactory interneurons emanates in the DBB including HDB. The centrifugal afferents from DBB extensively ramify in the entire OB, with highest neurite densities in the GL and the GCL. The respective synapses have, however, not been quantitatively assigned to the different layers in OB. These experiments conclusively demonstrate that both PGCs and GC are monosynaptically innervated from DBB, with the highest density of these centrifugally projecting neurons located in HDB. These results suggest that, besides the neuromodulatory, acetocholine-expressing neuronal population in HDB, a large population of projection neurons emanating from the entire DBB innervating the OB is of classical GABA/glutamatergic origin. Moreover, the relative contribution from DBB, in terms of neuron numbers that form synaptic contacts with common postsynaptic source interneurons in OB, is larger compared to that of centrifugal glutamatergic projection neurons originating in PC.

The fact that the OB receives a combination of centrifugal neuromodulatory inputs and classical GABA/glutamatergic synapses might suggest a heterosynaptic modulation model in which pairing of neuromodulator release and simultaneous synaptic activation may result in heterosynaptic modulation (Bailey et al., 2000). The release of neuromodulators would take place over a wide area within the bulb and thus their effects would involve diverse sets of synapses activated at the same time. Such a scenario could be advantageous for fast olfactory learning (Bailey et al., 2000).

Interestingly, besides AON, PC, and DBB, other brain nuclei or stray neurons scattered in other brain regions that are

(F) Optical section through the GCL of the OB. White arrows point at rAAV-infected, RABV-infected and coinfected PGCs.

(G) Optical section (EGFP channel) through the PC revealing bright fluorescent neurons.

(H) Optical section (EGFP channel) through HDB revealing numerous brightly fluorescent neurons.

See also Figures S5, S6, and S7 and Movie S2. GCs, granule cells; PGCs, periglomerular cells.

synaptically connected to bulbar interneurons were not detected. Neuromodulatory fibers releasing norepinephrine or serotonin (5HT) also elaborately innervate, and ramify in, the OB (McLean et al., 1989; Shipley et al., 1985; McLean and Shipley, 1987). These fibers contain numerous varicosities along their length, and their cell bodies reside in the locus coeruleus (LC) and the dorsal and median raphe nuclei, respectively (Matsutani and Yamamoto, 2008). Since no backlabeled neurons in LC or in the raphe nuclei could be detected, it seems likely that these neuromodulatory nuclei do not contain neurons monosynaptically connected with OB interneurons, which form classical GABA or glutamatergic synapses.

Limitations Regarding Specificity of Transsynaptic RABV Transport

Although powerful, virus-mediated transsynaptic tracing, as used here, has certain unresolved issues. Although transsynaptic transport of RABV is synapse specific, it is not clear if it is equally efficient across the different types of synapses (Ugolini, 1995, 2010). It is not known to what extent RABV crosses functionally active synapses more efficiently than functionally silent synapses, making an absolute quantification of synaptically connected neurons difficult. Unfortunately, this possibility of bias in transsynaptic transport applies to all transsynaptic-labeling techniques. However, the analysis presented here aims at a comparison of neuronal populations transsynaptically connected to a "common" postsynaptic source cell population. We therefore surmise that synapses, either GABA or glutamatergic, onto a common population of postsynaptic source neurons are unlikely to show a bias in transsynaptic transport. Notably, no other method available to date can identify cells in vivo that are retrogradely and monosynaptically connected to a source cell population of interest, over long distances, with the efficacy achieved by the approach presented here. Furthermore, there are no data available that show evidence for a bias in RABV-mediated transsynaptic traversal, except as discussed for the traversal of dendrodendritic, reciprocal synapses (see Extended Discussion and Figure S7).

EXPERIMENTAL PROCEDURES

Sample Preparation

Virus-injected mice (~8 weeks old) were anaesthetized with a mixture of ketamine and xylazine (100 mg/kg and 10 mg/kg, respectively; Atarost, Twistringen, Germany) injected intraperitoneally, and transcardially perfused with an ice-cold solution of 4% paraformaldehyde (PFA) in PBS. Brains were removed and postfixed at 4°C in 4% PFA for at least 15 hr. Fixed brains were then subjected to a modified clearing procedure, allowing for maximal preservation of the fluorophores (G.G., M.K.S., Annemarie Scherbarth, Ling Zhang, Izumi Fukunaga, Johann Engelhardt, Patrick Theer, Tyler Cutforth, Rolf Sprengel, unpublished data). Briefly, brains were washed in PBS three times for 1 hr each before dehydration with 1-propanol. Dehydration was performed at 25°C with 1-propanol/water mixtures at a pH of 9.5 in increasing 1-propanol concentrations (v/v). The single steps are 24 hr each in 30%, 50%, 70%, 80%, 96%, and 100%, then again for 24 hr in 100%. Optical clearing was performed by incubation in BABB (Dodt et al., 2007) with the pH adjusted to 9.5 for 16 hr at 25°C, followed by renewing the clearing solution and incubating for another 2 hr at room temperature (RT) or 80 hr at 4°C. All animal experiments were conducted under the license 35-915.81/G171/10 at the regional council in Karlsruhe and are in accordance with the guidelines of the Max Planck Society.

Microscopy

Light-sheet fluorescence microscopy was done using a custom-built microscope (G.G., M.K.S., A. Scherbarth, L. Zhang, I. Fukunaga, J. Engelhardt, P. Theer, T. Cutforth, and R. Sprengel, unpublished data), with custom mosaic acquisition software developed with Labview 8.6. Briefly, samples are illuminated from the side by a light sheet, which is accomplished by directing a laser (488 nm Sapphire, 649 nm Diode; Coherent, Dieburg, Germany; 514 nm Fandango; Cobolt, Stockholm, Sweden) over two scanners. The first scanner, in combination with the illumination objective, generates the light sheet (Keller and Stelzer, 2008), the second scanner is located between the first scanner and the illumination objective and rotates the light sheet to suppress shadow generation. The light sheet is focused on the sample using either a Leica MacroFluo 1.0× or 2.0× (Leica Microsystems, Wetzlar, Germany) as an illumination objective. Images are recorded using a charge-coupled device camera (Sensicam, PCO, Kelheim, Germany) located behind a detection objective (Leica HCX Apo L 10×/0.3W or Leica MacroFluo 0.8×), a motorized fluorescence emission filter wheel and a tube lens (Leica 202 mm, Linos 120 mm; Rodenstock, München, Germany, or Nikon 105 mm; Nikon, Tokyo, Japan). Motorized stages move the sample in x, y, and z to record mosaic images. Epifluorescence images were recorded using an Axioplan 2 (Carl Zeiss, Wetzlar, Germany); confocal images were recorded using Leica SP2 and SP5 microscopes, respectively.

Image Processing

To stitch the resulting mosaic images, an LSFM "Stitch Viewer" was developed as a plug-in for "ImageJ" that allows us to browse the data sets generated by the custom LSFM and pass them to Stefan Preibisch's stitching plug-ins (Preibisch et al., 2009) with options to set the linear overlap and linear shift of the tiles in x and y direction. If necessary, the position of each individual tile can be manually adjusted until a perfect overlap is reached. The plug-in also allows x and y-dependent z-corrections to compensate for misaligned light sheets and offers a "brightness alignment," which subtracts a fraction of a blurred version from the original image to reduce the brightness of overly bright areas. It also allows us to set z-dependent minimum and maximum brightness values and offers a user-configurable crosstalk compensation. The results of parameter changes on the stitched image are shown instantly, and it is possible to view data sets much larger than the computer's memory since only the currently active image plane is loaded into the RAM. Image planes are internally sorted and identified using a special file-naming scheme and metadata file unique to our microscope. The tiles are stitched and exported by passing them to Stefan Preibisch's stitching plug-ins (Preibisch et al., 2009), which can simply blend the images (using the previously set stitching parameters), or attempt to further optimize tile placement.

The resulting images were then 3D rendered using Amira 5.4.1. Counting of cells was done with the "Cell Counter" Plug-in developed by Kurt De Vos (see http://rsbweb.nih.gov/ij/plugins/cell-counter.html).

For details on experimental procedures concerning rehydratation of LSFM cleared brain preparations, immunohistochemistry, virus cloning/production, and surgical procedures, please see Extended Experimental Procedures.

SUPPLEMENTAL INFORMATION

Supplemental Information includes an Extended Discussion, Extended Experimental Procedures, seven figures, and two movies and can be found with this article online at http://dx.doi.org/10.1016/j.celrep.2012.10.008.

LICENSING INFORMATION

ACKNOWLEDGMENTS

The authors are indebted to Peter H. Seeburg for continuous scientific discussions and suggestions, critical reading of the manuscript and generous

financial support during the course of this work. We would also like to thank Troy Margrie, Winfried Denk, and Heinrich Betz for helpful comments on the manuscript. We would like to thank Annemarie Scherbarth, Judith Müller, Horst Grosskurt, Sabine Grünewald, and Nadin Hagendorf for excellent technical assistance and Nico Wieder, Steffen Illig, and Christian Kieser for their work on implementing the LSFM control software. Special thanks to Johanna Kolterman and Simon Wdowik for excellent stereotaxic virus injections and Anja Schmaltz for proofreading of the manuscript. This work was supported by the Max Planck Society and grants SCHW 1578/1-1 by the DFG to M.K.S. and SFB 870 to K.-K.C.

Received: March 5, 2012
Revised: August 30, 2012
Accepted: October 11, 2012
Published: November 8, 2012

REFERENCES

Astic, L., Saucier, D., Coulon, P., Lafay, F., and Flamand, A. (1993). The CVS strain of rabies virus as transneuronal tracer in the olfactory system of mice. Brain Res. *619*, 146–156.

Aungst, J.L., Heyward, P.M., Puche, A.C., Karnup, S.V., Hayar, A., Szabo, G., and Shipley, M.T. (2003). Centre-surround inhibition among olfactory bulb glomeruli. Nature *426*, 623–629.

Bailey, C.H., Giustetto, M., Huang, Y.Y., Hawkins, R.D., and Kandel, E.R. (2000). Is heterosynaptic modulation essential for stabilizing Hebbian plasticity and memory? Nat. Rev. Neurosci. *1*, 11–20.

Bak, I.J., Markham, C.H., Cook, M.L., and Stevens, J.G. (1977). Intraaxonal transport of Herpes simplex virus in the rat central nervous system. Brain Res. *136*, 415–429.

Balu, R., Pressler, R.T., and Strowbridge, B.W. (2007). Multiple modes of synaptic excitation of olfactory bulb granule cells. J. Neurosci. *27*, 5621–5632.

Beier, K.T., Saunders, A., Oldenburg, I.A., Miyamichi, K., Akhtar, N., Luo, L., Whelan, S.P., Sabatini, B., and Cepko, C.L. (2011). Anterograde or retrograde transsynaptic labeling of CNS neurons with vesicular stomatitis virus vectors. Proc. Natl. Acad. Sci. USA *108*, 15414–15419.

Bohland, J.W., Wu, C., Barbas, H., Bokil, H., Bota, M., Breiter, H.C., Cline, H.T., Doyle, J.C., Freed, P.J., Greenspan, R.J., et al. (2009). A proposal for a coordinated effort for the determination of brainwide neuroanatomical connectivity in model organisms at a mesoscopic scale. PLoS Comput. Biol. *5*, e1000334.

Braz, J.M., Rico, B., and Basbaum, A.I. (2002). Transneuronal tracing of diverse CNS circuits by Cre-mediated induction of wheat germ agglutinin in transgenic mice. Proc. Natl. Acad. Sci. USA *99*, 15148–15153.

Carson, K.A. (1984a). Localization of acetylcholinesterase-positive neurons projecting to the mouse main olfactory bulb. Brain Res. Bull. *12*, 635–639.

Carson, K.A. (1984b). Quantitative localization of neurons projecting to the mouse main olfactory bulb. Brain Res. Bull. *12*, 629–634.

Cowan, W.M. (1998). The emergence of modern neuroanatomy and developmental neurobiology. Neuron *20*, 413–426.

Cullinan, W.E., and Záborszky, L. (1991). Organization of ascending hypothalamic projections to the rostral forebrain with special reference to the innervation of cholinergic projection neurons. J. Comp. Neurol. *306*, 631–667.

Dodt, H.U., Leischner, U., Schierloh, A., Jährling, N., Mauch, C.P., Deininger, K., Deussing, J.M., Eder, M., Zieglgänsberger, W., and Becker, K. (2007). Ultramicroscopy: three-dimensional visualization of neuronal networks in the whole mouse brain. Nat. Methods *4*, 331–336.

Enquist, L.W., Miselis, R.R., and Card, J.P. (1994). Specific infection of rat neuronal circuits by pseudorabies virus. Gene Ther. *1*(*Suppl 1*), S10.

Gao, Y., and Strowbridge, B.W. (2009). Long-term plasticity of excitatory inputs to granule cells in the rat olfactory bulb. Nat. Neurosci. *12*, 731–733.

Helmchen, F., and Denk, W. (2005). Deep tissue two-photon microscopy. Nat. Methods *2*, 932–940.

Helmstaedter, M., Briggman, K.L., and Denk, W. (2008). 3D structural imaging of the brain with photons and electrons. Curr. Opin. Neurobiol. *18*, 633–641.

Horowitz, L.F., Montmayeur, J.P., Echelard, Y., and Buck, L.B. (1999). A genetic approach to trace neural circuits. Proc. Natl. Acad. Sci. USA *96*, 3194–3199.

Isaacson, J.S. (2010). Odor representations in mammalian cortical circuits. Curr. Opin. Neurobiol. *20*, 328–331.

Jach, G., Pesch, M., Richter, K., Frings, S., and Uhrig, J.F. (2006). An improved mRFP1 adds red to bimolecular fluorescence complementation. Nat. Methods *3*, 597–600.

Kasa, P., Hlavati, I., Dobo, E., Wolff, A., Joo, F., and Wolff, J.R. (1995). Synaptic and non-synaptic cholinergic innervation of the various types of neurons in the main olfactory bulb of adult rat: immunocytochemistry of choline acetyltransferase. Neuroscience *67*, 667–677.

Katz, L.C., Burkhalter, A., and Dreyer, W.J. (1984). Fluorescent latex microspheres as a retrograde neuronal marker for in vivo and in vitro studies of visual cortex. Nature *310*, 498–500.

Keller, P.J., and Stelzer, E.H. (2008). Quantitative in vivo imaging of entire embryos with Digital Scanned Laser Light Sheet Fluorescence Microscopy. Curr. Opin. Neurobiol. *18*, 624–632.

Kim, J.S., Enquist, L.W., and Card, J.P. (1999). Circuit-specific coinfection of neurons in the rat central nervous system with two pseudorabies virus recombinants. J. Virol. *73*, 9521–9531.

Kiselycznyk, C.L., Zhang, S., and Linster, C. (2006). Role of centrifugal projections to the olfactory bulb in olfactory processing. Learn. Mem. *13*, 575–579.

Kissa, K., Mordelet, E., Soudais, C., Kremer, E.J., Demeneix, B.A., Brûlet, P., and Coen, L. (2002). In vivo neuronal tracing with GFP-TTC gene delivery. Mol. Cell. Neurosci. *20*, 627–637.

Köbbert, C., Apps, R., Bechmann, I., Lanciego, J.L., Mey, J., and Thanos, S. (2000). Current concepts in neuroanatomical tracing. Prog. Neurobiol. *62*, 327–351.

Li, A., Gong, H., Zhang, B., Wang, Q., Yan, C., Wu, J., Liu, Q., Zeng, S., and Luo, Q. (2010). Micro-optical sectioning tomography to obtain a high-resolution atlas of the mouse brain. Science *330*, 1404–1408.

Lo, L., and Anderson, D.J. (2011). A Cre-dependent, anterograde transsynaptic viral tracer for mapping output pathways of genetically marked neurons. Neuron *72*, 938–950.

Lundh, B. (1990). Spread of vesicular stomatitis virus along the visual pathways after retinal infection in the mouse. Acta Neuropathol. *79*, 395–401.

Luo, L., Callaway, E.M., and Svoboda, K. (2008). Genetic dissection of neural circuits. Neuron *57*, 634–660.

Matsutani, S. (2010). Trajectory and terminal distribution of single centrifugal axons from olfactory cortical areas in the rat olfactory bulb. Neuroscience *169*, 436–448.

Matsutani, S., and Yamamoto, N. (2008). Centrifugal innervation of the mammalian olfactory bulb. Anat. Sci. Int. *83*, 218–227.

McLean, J.H., and Shipley, M.T. (1987). Serotonergic afferents to the rat olfactory bulb: I. Origins and laminar specificity of serotonergic inputs in the adult rat. J. Neurosci. *7*, 3016–3028.

McLean, J.H., Shipley, M.T., Nickell, W.T., Aston-Jones, G., and Reyher, C.K. (1989). Chemoanatomical organization of the noradrenergic input from locus coeruleus to the olfactory bulb of the adult rat. J. Comp. Neurol. *285*, 339–349.

Miyamichi, K., Amat, F., Moussavi, F., Wang, C., Wickersham, I., Wall, N.R., Taniguchi, H., Tasic, B., Huang, Z.J., He, Z., et al. (2011). Cortical representations of olfactory input by trans-synaptic tracing. Nature *472*, 191–196.

Mouret, A., Murray, K., and Lledo, P.M. (2009). Centrifugal drive onto local inhibitory interneurons of the olfactory bulb. Ann. N Y Acad. Sci. *1170*, 239–254.

Osakada, F., Mori, T., Cetin, A.H., Marshel, J.H., Virgen, B., and Callaway, E.M. (2011). New rabies virus variants for monitoring and manipulating activity and gene expression in defined neural circuits. Neuron *71*, 617–631.

Pignatelli, A., and Belluzzi, O. (2008). Cholinergic modulation of dopaminergic neurons in the mouse olfactory bulb. Chem. Senses *33*, 331–338.

Preibisch, S., Saalfeld, S., and Tomancak, P. (2009). Globally optimal stitching of tiled 3D microscopic image acquisitions. Bioinformatics *25*, 1463–1465.

Ragan, T., Kadiri, L.R., Venkataraju, K.U., Bahlmann, K., Sutin, J., Taranda, J., Arganda-Carreras, I., Kim, Y., Seung, H.S., and Osten, P. (2012). Serial two-photon tomography for automated ex vivo mouse brain imaging. Nat. Methods *9*, 255–258.

Rancz, E.A., Franks, K.M., Schwarz, M.K., Pichler, B., Schaefer, A.T., and Margrie, T.W. (2011). Transfection via whole-cell recording in vivo: bridging single-cell physiology, genetics and connectomics. Nat. Neurosci. *14*, 527–532.

Shipley, M.T., Halloran, F.J., and de la Torre, J. (1985). Surprisingly rich projection from locus coeruleus to the olfactory bulb in the rat. Brain Res. *329*, 294–299.

Sosulski, D.L., Bloom, M.L., Cutforth, T., Axel, R., and Datta, S.R. (2011). Distinct representations of olfactory information in different cortical centres. Nature *472*, 213–216.

Strowbridge, B.W. (2009). Role of cortical feedback in regulating inhibitory microcircuits. Ann. N Y Acad. Sci. *1170*, 270–274.

Swanson, L.W. (2000). Cerebral hemisphere regulation of motivated behavior. Brain Res. *886*, 113–164.

Ugolini, G. (1995). Specificity of rabies virus as a transneuronal tracer of motor networks: transfer from hypoglossal motoneurons to connected second-order and higher order central nervous system cell groups. J. Comp. Neurol. *356*, 457–480.

Ugolini, G. (2010). Advances in viral transneuronal tracing. J. Neurosci. Methods *194*, 2–20.

Wickersham, I.R., Finke, S., Conzelmann, K.K., and Callaway, E.M. (2007a). Retrograde neuronal tracing with a deletion-mutant rabies virus. Nat. Methods *4*, 47–49.

Wickersham, I.R., Lyon, D.C., Barnard, R.J., Mori, T., Finke, S., Conzelmann, K.K., Young, J.A., and Callaway, E.M. (2007b). Monosynaptic restriction of transsynaptic tracing from single, genetically targeted neurons. Neuron *53*, 639–647.

Willhite, D.C., Nguyen, K.T., Masurkar, A.V., Greer, C.A., Shepherd, G.M., and Chen, W.R. (2006). Viral tracing identifies distributed columnar organization in the olfactory bulb. Proc. Natl. Acad. Sci. USA *103*, 12592–12597.

Wilson, R.I., and Mainen, Z.F. (2006). Early events in olfactory processing. Annu. Rev. Neurosci. *29*, 163–201.

Yoshihara, Y., Mizuno, T., Nakahira, M., Kawasaki, M., Watanabe, Y., Kagamiyama, H., Jishage, K., Ueda, O., Suzuki, H., Tabuchi, K., et al. (1999). A genetic approach to visualization of multisynaptic neural pathways using plant lectin transgene. Neuron *22*, 33–41.